Int. J. Heat Mass Transfer. Vol. 36, No. 9, pp. 2327–2337, 1993
Printed in Great Britain

0017 9310/93 $6.00+0.00

Experimental investigations of heat transfer enhancement and flow losses in a channel with double rows of longitudinal vortex generators

ST. TIGGELBECK, N. K. MITRA and M. FIEBIG
Institut für Thermo- und Fluiddynamik, Ruhr-Universität Bochum, D-4630 Bochum, F.R.G.

(*Received* 12 *June* 1991 *and in final form* 20 *March* 1992)

Abstract—Flow structure, heat transfer, and drag by longitudinal vortices generated by double rows of delta winglets in transition channel flow are investigated for the reduction of the gas side heat transfer resistance of compact heat exchangers. The experiments consist of flow visualization by laser light sheets, liquid crystal thermography for local heat transfer and balance measurements for drag. Angle of attack and channel Reynolds number have been varied. Aligned delta winglet double rows show higher heat transfer enhancement than staggered. The critical angle of attack for the formation of longitudinal vortices is smaller behind the second row than behind the first. Heat transfer enhancements of 80% and drag increases of 160% have been found on wall areas 40 times the winglet area. The ratio of heat transfer enhancement and drag increase is larger for higher Reynolds numbers.

INTRODUCTION

COMPACT heat exchangers are used in many different applications, so their performance improvement with respect to the reduction of manufacturing costs by using less material or with respect to the reduction of operating costs by reducing energy losses is of great technical, economical, and, not least, of ecological importance. This need for performance improvement becomes especially necessary in heat exchangers for gases, for example in fin-tube heat exchangers (Fig. 1), since the heat transfer resistance for gases is 10–50 times larger than for liquids because of smaller density and thermal conductivity of the gases.

Normally the gas side heat transfer surface is enlarged to compensate for the low heat transfer characteristic. Typical values for the gas side heat transfer surface per unit volume of heat exchanger are 700–1000 $m^2\ m^{-3}$ [1]. This results in low hydraulic diameters (of a few millimeters) on the gas side. In spite of the much larger heat transfer area on the gas side, the higher heat transfer resistance for such equipment still lies on the gas side. So for performance enhancement of such heat exchangers the gas side thermal resistance needs to be further reduced.

A large number of methods for the increase of gas side heat transfer has been described by Kays and London [1]. Most of the described methods deal with geometrical modifications of the gas side heat transfer surface such as roughness elements, turbulators, or secondary fins to structure the flow and temperature field. In ref. [1] experimental data for average heat transfer and pressure loss of some of these modifications are presented.

The present work is concerned with experimental investigations on the influence of longitudinal vortices on heat transfer and drag of compact heat exchangers. The longitudinal vortices are generated by small delta winglets (delta half wings) on the heat transfer surfaces. These winglets are punched out of the fin (see Fig. 2). While remaining attached to the fin at their chord, the delta winglets stick out in the flow field with an angle to the main flow direction. The flow separates at the leading edges of the winglets and forms stable longitudinal vortices in their wake. The swirling motion of the vortices enhances the exchange of fluid between the wall and core regions and increase the heat transfer.

Edwards and Alker [2] compared the influence of rows of cubes and delta winglet vortex generators for heat transfer enhancement between parallel plates. They found that delta winglets which produce counter-rotating longitudinal vortices gave the best heat transfer enhancement. It was locally not as high as for the cubes but persisted much further downstream.

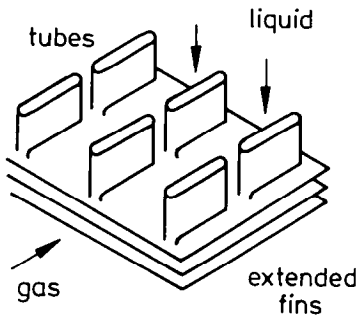

FIG. 1. Schematic of compact heat exchanger with flat tubes (liquid flow) and extended fins (gas flow).

NOMENCLATURE

A_f	fin area [m^2]
A_{VG}	vortex generator area [m^2]
a	temperature conductivity of air [m^2 s^{-1}]
B	investigated channel width [m]
Bi	Biot number, $\alpha\delta/\lambda$
$b/2$	vortex generator height [m]
c_f	heat capacity of fin material [J (kg K)$^{-1}$]
D_h	hydraulic diameter, $2H$ [m]
H	channel height [m]
L	channel length [m]
l	winglet chord [m]
Nu	Nusselt number, $\alpha D_h/\lambda$
Nu_x	span averaged Nusselt number
Re	Reynolds number, UD_h/ν
Pr	Prandtl number, ν/a
t	heating time [s]
T_a	air temperature [°C]
T_f	wall temperature [°C]
T_{fo}	initial wall temperature before heating [°C]
T_{LC}	indication temperature of liquid crystal coating [°C]
Tu_x	turbulence level of main flow direction $(u'^2)^{1/2}/U$
U	mean flow velocity [m s^{-1}]
u'	fluctuation component of u_x
u_x	flow component to main flow direction [m s^{-1}]
x_v	distance from channel leading edge [m]
x, y, z	coordinates [m]
x^*	parameter of similarity, $x/(D_h RePr)$
Δy	spanwise distance of the centerline of 1 and 2 row winglet pair [m].

Greek symbols

α	heat transfer coefficient [W (m^2 K)$^{-1}$]
α	kinetic energy correction factor
β	angle of attack [ ]
β	momentum correction factor
δ	fin thickness [m]
Λ	winglet aspect ratio, $2b/l$
λ	wavelength [m]
λ_f	thermal conductivity of fin material [W (m^2 K)$^{-1}$]
ν	kinematic viscosity of air [m^2 s^{-1}]
ρ_f	density of fin material [kg m^{-3}].

Co-rotating longitudinal vortices were not effective. Russell *et al.* [3] made some basic investigations on different types of vortex generators which were mounted on, punched out, or stamped out of the channel wall. They found rectangular winglets to give highest heat transfer. They also investigated arrays of two staggered rows of winglets in close configuration. The second row they found to be a 'booster' because it enhanced the span averaged heat transfer further over the enhancement of the first row alone.

Fiebig *et al.* [4] showed from numerical investigations that wings as well as half wings (winglets) in channel flows produce high heat transfer enhancements which can reach a factor of '3' over the heat transfer in a channel without vortex generator. The heat transfer increases with Reynolds number and angle of attack in the considered ranges ($Re \leqslant 4000$, $\beta \leqslant 50°$).

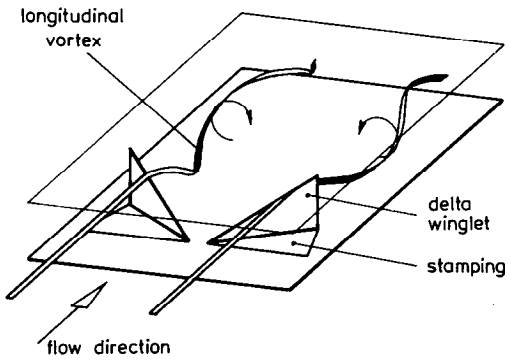

FIG. 2. Delta winglet pair punched out of a channel wall with longitudinal vortex formation.

Turk and Junkhan [5] experimentally investigated pairs of rectangular winglets which produce counter-rotating longitudinal vortices on a flat plate. They found that the ratio of the spanwise averaged Nusselt number normalized with the corresponding flat plate value increased with streamwise distance. This means that the heat transfer augmentation due to the vortices does not decrease as fast as the heat transfer on a flat plate.

Fiebig *et al.* ([6, 7]) have measured mean heat transfer enhancements of up to 60% at $Re_H = UH/\nu = 1360$ with a single delta wing at large angles of attack ($\beta = 50°$) in a rectangular channel. The ratio of wing to fin area in this experiment is 0.02.

Tiggelbeck *et al.* [8] investigated delta winglet pairs in single and aligned double-row arrangement at angles of attack of $\beta = 45°$. They found streamwise distances of 7–10 channel heights between the vortex generator rows to give highest local and average heat transfer. The local heat transfer peaks behind the second row have been higher than behind the first row.

Apart from the work of Russell *et al.* [3] and of Tiggelbeck *et al.* [8], all the previous investigations deal with the effects resulting from single or spanwise rows of vortex generators. In heat exchanger applications with ratios of flow length to channel height

L/H of at least 30, large heat transfer will require not one but several rows of vortex generators. The streamwise arrangement of different rows will be of great importance because the oncoming flow to the vortex generators in the rear will be of higher turbulence, vorticity, and inhomogeneity.

The purpose of the present study is an experimental investigation of flow structure and heat transfer in a channel built by parallel plates with two rows of longitudinal vortex generators with aligned or staggered arrangement. The comparison of the results of aligned and staggered rows will elucidate the changing interaction of the vortex generators and the influence of inhomogeneous oncoming flow. The present work is complementary to ref. [8] which presented only heat transfer enhancement due to two in-line rows of vortex generators. In the present work both heat transfer and drag (for flow losses) are examined for two staggered rows of vortex generators and compared with those for the in-line arrangement.

EXPERIMENTAL METHODS AND FACILITIES

Windtunnel

The experiments are performed in a small wind tunnel (see Fig. 3), with a vertical test section of dimensions of $160 \times 320 \times 800$ mm^3 (width × depth × length). The mean flow velocity U in the test section can be varied from 0.4 to 4 m s^{-1}. The air can be heated electrically from room temperature (20–22°C) to 50°C. Local velocity deviations of ±3% from the mean velocity occur in the velocity range given above in a central cross-sectional area of 120×240 mm^2 at the test section entrance. The temperature deviations for a mean temperature of about 50°C are of the order of 0.15°C for the central cross-sectional area given above. The measured turbulence level of the main flow component in the test section $Tu_x = (u_x'^2)^{1/2}/U$ is within 0.75 and 0.85% for the whole velocity range. Closed-circuit wind tunnel flow is used for thermal measurements where high air temperature is needed. For flow visualization open-circuit flow is used in order to prevent pollution of the wind tunnel by smoke or oil. Open-circuit flow is also used for drag measurements.

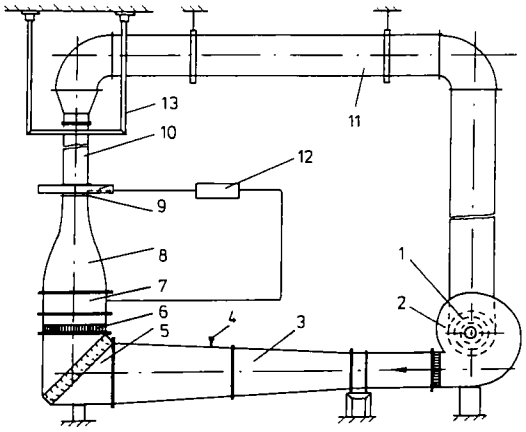

FIG. 3. Sketch of wind tunnel set-up.

Flow visualization

Tracer particles of evaporating glycerine are used for observations of the flow structure in the vortex generator wake. Cross-sections of the visible flow field are observed by laser light sheets. The flow visualizations are recorded on video tapes. The optical arrangement for the flow visualization and the systems for the evaporation of glycerine are sketched in Fig. 4. The glycerine is evaporated either by a modified smoke wire technique or directly at the model surface. The smoke wire is perpendicular to the main flow near the entrance cross-section of the vertical test section. Pulling the wire through a capillary filled with glycerine yields a uniform pattern of about five small glycerine droplets per centimeter wire length. Electrical heating of the wire leads to evaporation of the glycerine. The results are parallel smoke filaments in the flow. Better optical results and more detailed information about the flow structure are received by evaporation of glycerine directly at the model surface. For this purpose two thin pieces of black cardboard are pasted over the vortex generator surface with a wound constantan wire between them. The cardboard saturated with glycerine is heated electrically. The glycerine evaporates on the model surface and follows the flow separating at the edges of the vortex generators.

The optical assembly allows to position light sheets of variable thickness (1–3 mm) in the flow. Test section and model (except the test fin which is coated with black paint) are fabricated of transparent glass or polycarbonat.

Heat transfer measurements

Local heat transfer on the wall is measured by unsteady liquid crystal thermography. For this purpose the test configuration is unsteadily heated in a warm air flow within the test section. For a model consisting of a stack of parallel plates with vortex generators punched out of them, the temporal development of the temperature of one plate can be regarded as the response of a thin body to a sudden jump in the surrounding temperature. For heat transfer measurements the investigated plate area is divided into small elements as shown in Fig. 5.

The balance of heat fluxes in an element gives

$$\rho_f c_f \delta \, \mathrm{d}x \, \mathrm{d}y \frac{\partial T_f}{\partial t} = 2\alpha \, \mathrm{d}x \, \mathrm{d}y (T_a - T_f) + \lambda \delta \, \mathrm{d}x \, \mathrm{d}y \left\{ \frac{\partial^2 T_f}{\partial x^2} + \frac{\partial^2 T_f}{\partial y^2} \right\}. \quad (1)$$

Assuming steady, incompressible flow, negligible heat conduction along the wall, and constant temperature across the plate thickness, i.e. negligible tem-

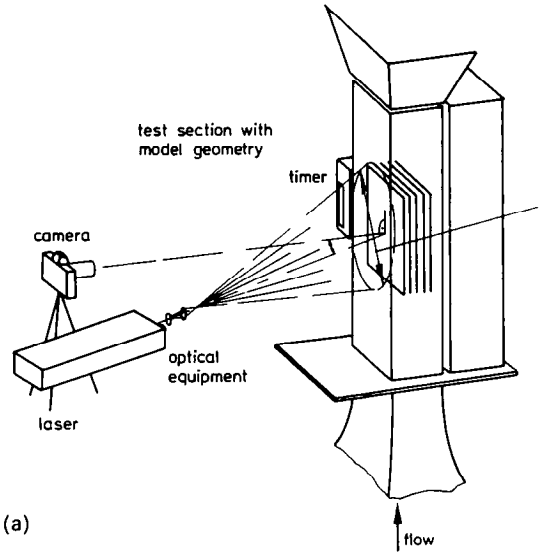

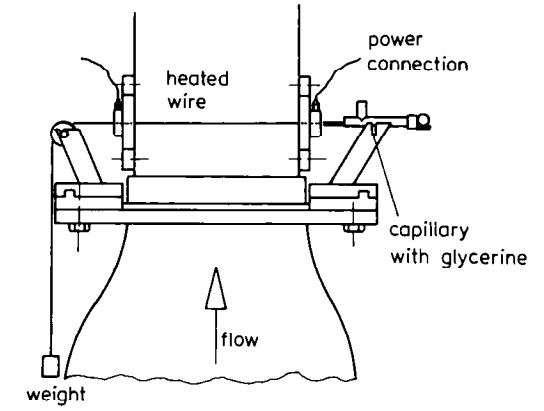

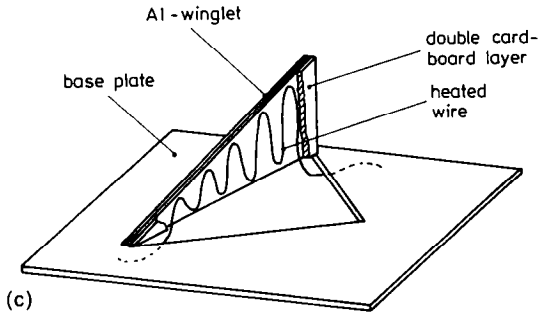

FIG. 4. (a) Optical configuration for flow visualization and smoke techniques, (b) smoke wire, (c) direct evaporation.

perature gradient in the z-direction, an equation for the local heat transfer coefficient α can be derived from equation (1) after integration:

$$\alpha = \frac{\rho_f c_f \delta}{2t(T_f)} \ln \frac{T_a - T_{fo}}{T_a - T_f}. \quad (2)$$

This equation gives the heat transfer coefficient locally averaged for the upper and lower sides of the plate. The term $t(T_f)$ stands for the time interval needed to heat up the element from its initial temperature T_{fo} to a temperature T_f. Only the relation between T_f and $t(T_f)$ has to be measured to determine α. The method represents the thermal boundary condition of constant wall temperature (T_f = const.) in a steady experiment [9]. The assumption of no temperature gradient across the plate thickness is valid for a small Biot modulus $Bi = \alpha\delta/\lambda_f$ which is of the order of 0.12 in our experiments with air flows. The second assumption of negligible heat conduction along the wall has been investigated numerically by the present group for different wall conditions. The computations show that for thin walls of low thermal conductivity significant heat conduction occurs only at positions where the distribution of heat transfer coefficients has local extrema with large second derivatives. There experimental errors due to the heat conduction can become up to 10%. These areas with significant error in α are, however, small compared to the investigated model surface area (of the order of 2–3%). So even with the error in local α due to conduction along the plate, the error in the average heat transfer coefficient over the total area will be negligible. The assumption to be fulfilled for negligible heat conduction along the fin is that the ratio $(T_{f,C} - T_{fo})/(T_a - T_{fo})$ is small. For the present case it was about 0.3.

The unsteady local surface temperature of the test geometry during the heating phase is determined by means of a thin coating of encapsulated thermochromic liquid crystals (TLC) which is sprayed onto the test surface by an air brush. TLC have the property to reflect incident light at some specified temperature. The relation between temperature and reflected wavelength is known. The response time of TLC to temperature changes is of the order of 20–50 ms. They yield the temporal development of a whole surface. They are relatively cheap, easy to use and show good temperature and spatial resolution. The TLC used for the present study show visible reflection within the temperature range of 29.5–30.5°C. In order to increase the contrast of reflection the model surface is blackened with a pale paint before being coated

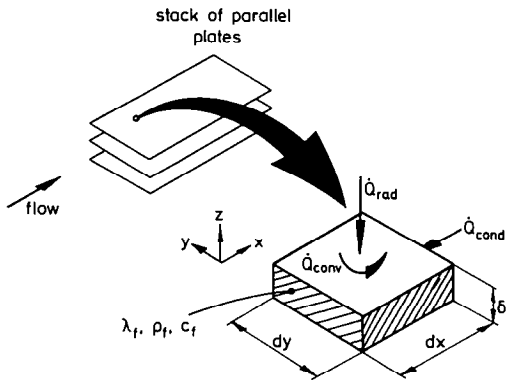

FIG. 5. Heat fluxes for elements of the test model.

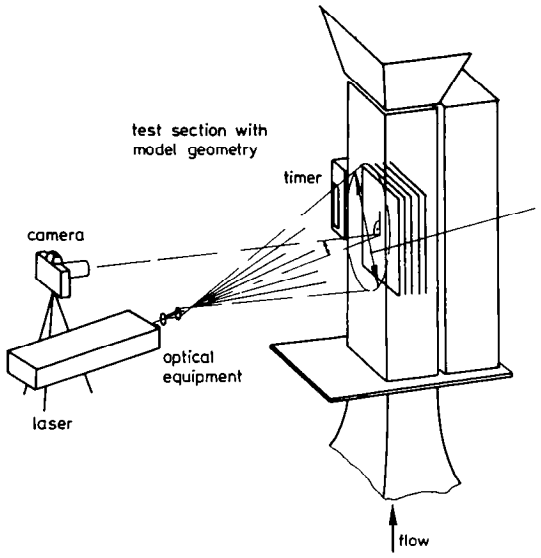

FIG. 6. Experimental configuration for heat transfer measurements by unsteady liquid crystal thermography.

with TLC. The experimental configuration is shown in Fig. 6.

In the measurement procedure first a warm air flow ($T_a = 50°C$) is established in the test section of the wind tunnel. Then the model—initially at room temperature T_{fo}—is slid in the warm air stream, where it is illuminated by monochromatic laser light ($\lambda = 514$ nm). The model is heated up from room temperature to the air flow temperature. The green laser light is reflected by the TLC coating from those points of the surface where the temperature T_f becomes equal to $T_{LC} = 30.0°C$. In this way the temporal development of the 30.0°C-isotherms can be observed on the model surface. These isotherms are recorded either by means of a series of photos or on a video tape. The locations of the isotherms, visible on the respective recording as isochromatics of higher grey level than the black model surface, can be digitalized and local heat transfer can be computed for the model surface.

The RSS-uncertainty described by Moffat [10] can be calculated by the uncertainties of the experimental data (see Table 1). It is given by

$$\partial\alpha = \left[\sum\left(\frac{\partial\alpha}{\partial X_i}\mathrm{d}X_i\right)^2\right]^{1/2} \tag{3}$$

Table 1. Tolerance of experimental variables

Air temperature	T_a	0.2 K
Fin temperature	T_{fo}	0.2 K
Indication temperature of TLC coating	T_{LC}	0.1 K
Plate thickness	δ	0.02 mm
Heating time	t	0.1 s
Velocity of air flow	U	3%
Thermophys. prop. of fin material and air	ρ, c, λ	Negligible

where X_i stands for the different experimental variables describing α, and $\mathrm{d}X_i$ is the tolerance of the corresponding variables. The resulting total RSS-value for a local heat transfer coefficient α calculated from equation (2) is 6.3% and 2.65% for heating times of 10 and 30 s, respectively. These times are typical TLC indication times for low and high heat transfer. The measurement of local heat transfer can be reproduced with an accuracy of a few percent. The Reynolds number of the flow can be adjusted with an accuracy of about 3%.

Drag measurements

Because of the very low pressure drops in the test configurations (of the order of 10^{-2} Pa), the additional flow losses due to the vortex generators in the test configuration are determined by measuring the drag. The relation between the coefficients of drag, pressure drop, and dissipation can be derived from the equations of mechanical energy and momentum (see ref. [11]). It is given by

$$c_\psi = c_p\frac{H}{\Delta x} + \Delta\alpha\frac{H}{2\Delta x}; \quad c_F = c_p\frac{H}{2\Delta x} + \Delta\beta\frac{H}{\Delta x} \tag{4}$$

where H is the channel height and Δx the channel length. The coefficients are coupled by the correction factors for kinetic energy and momentum α and β:

$$\alpha = \frac{1}{U^3 A_F}\int v^2 v_x\,\mathrm{d}A_F; \quad \beta = \frac{1}{U^2 A_F}\int v_x^2\,\mathrm{d}A_F. \tag{5}$$

In the vertical test section the drag is determined by measuring the change of weight of a test configuration with and without vortex generators as well as with and without flow. The change represents the additional drag induced by the vortex generators. The test equipment is shown in Fig. 7.

The investigated test model area is separated from the other configuration. It is hung from a scale by means of thin wires. The influence of the wires on the test signal at the scale is taken into account by a separate experiment for each configuration.

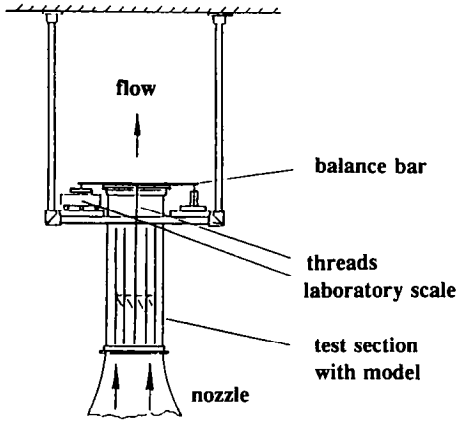

FIG. 7. Experimental set-up for drag measurements.

The RSS-value of the error for the drag forces and the drag coefficient c_F is 6.5%.

MODEL CONFIGURATIONS

The test model consists of a stack of parallel plates representing a part of the gas side fin arrangement of a compact heat exchanger (see Fig. 1). The vortex generators are punched and bent out of these plates (Fig. 8). Only symmetrical delta winglet pairs are used as vortex generators which can also serve as spacers of the plates. They are arranged in pairs so that they produce counter-rotating vortices. Large angles of attack, $\beta \geqslant 45^\circ$, are used. At least three parallel plates are taken in a stack. On each of these plates two rows of three winglet pairs in spanwise direction are punched out (Fig. 8). The measurements have been performed at the middle winglet pair of the middle plate. In this way symmetry conditions along the side edges of the investigated plate-fin area (dotted line in Fig. 8) as well as periodicity of the flow at the stampings of the winglets are assured. All plates except the test plate are made of transparent material to enable optical access.

Previous numerical studies [12] and flow visualization [3] noted a negative influence on the longitudinal vortex strength by suction (rear) side stampings. Hence in these experiments the stampings are made on the pressure side of the winglets. The channel height, the span of the investigated area, the ratio of the fin area to the vortex generator surface area, and the streamwise distance of the vortex generator rows are held constant. The streamwise distance has been investigated by the present group in previous investigations (see ref. [8]). The optimum value for maximum local and average heat transfer has been stated to about seven channel heights.

The reference case for the experiments is the flow in a plane duct. All constant and variable parameters of the investigations described here are listed in Table 2 and shown in Fig. 8.

RESULTS AND DISCUSSION

Qualitative flow structure

The flow structure at the wake of the vortex generators is strongly dependent on angle of attack and Reynolds number. It has been shown by Tiggelbeck *et al.* [8] that for single rows of vortex generators only at small Reynolds numbers $Re = UD_h/\nu \leqslant 1300$ a laminar longitudinal vortex appears. For higher Reynolds numbers the vortex grows turbulent with turbulence levels of the main flow component of more than 10 times the turbulence level of the homogeneous oncoming flow. This also holds for the wake of the second row of vortex generators. In ref. [8] it has also been shown that for high angles of attack there is no longitudinal vortex downstream of the delta winglets, the separating flow forms a recirculation zone. The critical angle of attack for a single row of delta winglets was found to be $\beta_{crit} \approx 70^\circ$. Investigations for second row delta winglets have shown similar behaviour. Figure 9 shows light sheets perpendicular to the main flow direction behind one delta winglet of the symmetrical pair for two angles of attack, $\beta = 45$ and 65° for aligned and staggered rows of vortex generators. The flow is observed parallel to the main flow direction from the back side of the channel. The $\beta = 45^\circ$ photographs, Fig. 9 (a) (aligned) and (b) (staggered), show the typical cross-sections of a longi-

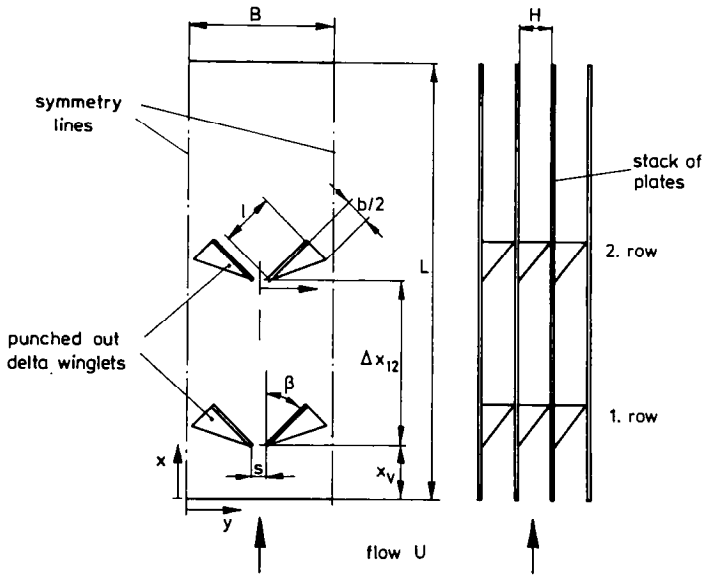

FIG. 8. Model geometry in the form of a stack of parallel plates with rows of delta winglet pairs punched out of each (see also Table 2).

Table 2. Geometrical and flow parameters of winglet configuration (see Fig. 8)

Channel configuration	
Constant	
Channel height	$H = 20$ mm
Width of symmetry area	$B = 5H$
Channel length	$L = 30H$
Vortex generator geometry	
Symmetrical delta winglet pair, pressure side stamping angle of attack	$\beta = 45^\circ, 65^\circ$
Winglet length	$l = 2H$
Winglet height	$b/2 = H$
Aspect ratio	$b^2/A_{VG} = 2$
Winglet tip distance	$s = 0.4H$
Streamwise position of first winglet row	$x_1 = H, 3H$
Streamwise distance between winglet rows	$\Delta x = 7H$
Variable	
Spanwise distance of winglet pair centerline	$\Delta y = 0, B/2$
Angle of attack	$\beta = 45^\circ, 65^\circ$
Reynolds number	$Re = 2000$–8000

tudinal vortex downstream of the second row of vortex generators. Besides the dominating primary vortex small secondary vortices resulting from entrainment effects and flow through the stamping of the vortex generator appear. At $\beta = 65^\circ$ the flow does not form a longitudinal vortex downstream of the second delta winglet row, even for aligned arrangement (Fig. 9(c)). The critical angle of attack for the second row is $\beta_{crit} \approx 55^\circ$. This is in contrast to the first row, where β_{crit} is 70° (Fig. 9(d)). The inhomogeneities and the

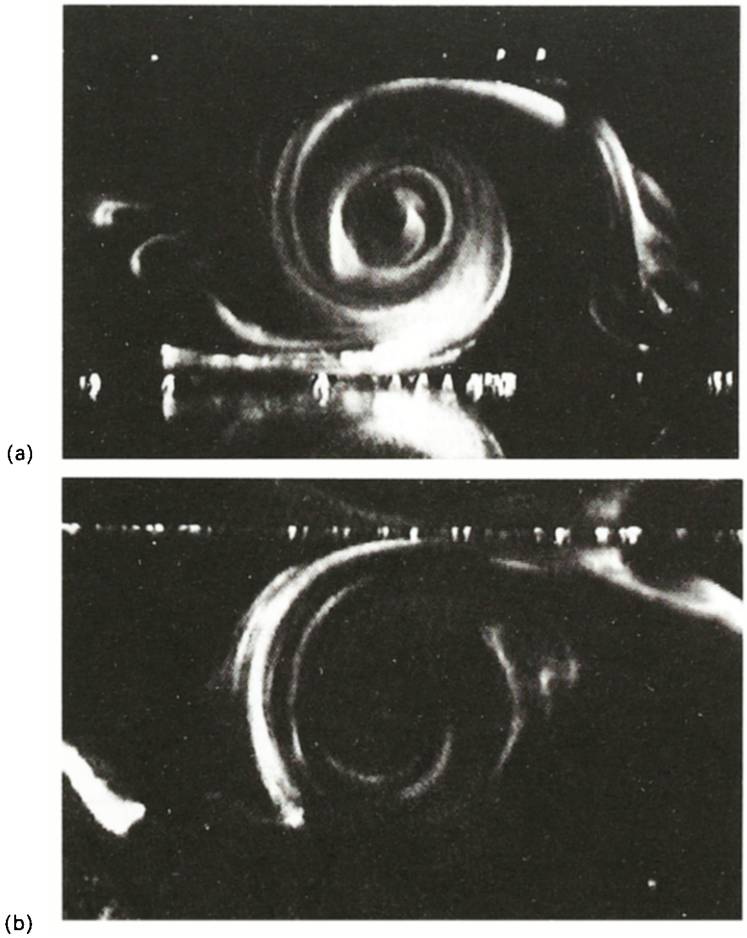

FIG. 9. Flow structure $x/H = 3.5$ downstream of a delta winglet (Table 2) for the second row at $\beta = 45^\circ$, (a) aligned, (b) staggered arrangement, (c) aligned arrangement for $\beta = 65^\circ$, (d) first row at $\beta = 65^\circ$, $Re = 1300$.

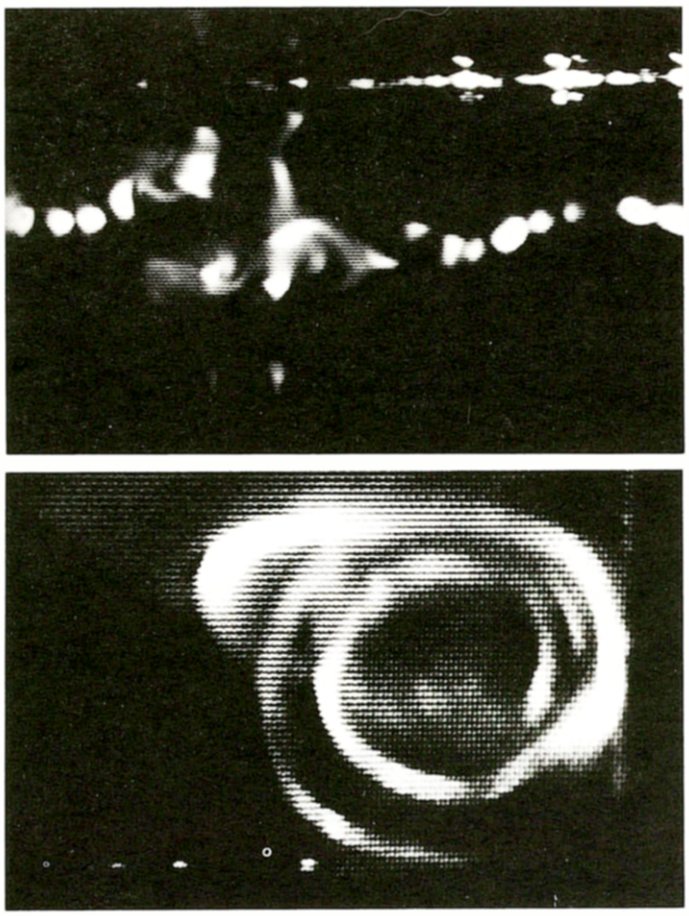

FIG. 9.—*Continued.*

higher turbulence level of the oncoming flow of the second row probably are the reasons for this.

The flow structures behind the second row for staggered or aligned arrangement of the two rows are qualitatively similar, no distinct influence of the row configuration can be found. Behind the second row the flow is slightly more unsteady than behind the first row.

For supercritical flow ($\beta \geqslant 55^\circ$) a recirculation zone of separated flow is formed behind the winglets as can also be seen behind the first row for supercritical flow.

Local heat transfer

The local heat transfer is effectively increased by the longitudinal vortices. Figure 10 shows the local heat transfer coefficient at the channel wall with two pairs of delta winglets in staggered arrangement with $\Delta y = B/2$, $Re = 4600$ and $\beta = 45^\circ$. Local heat transfer

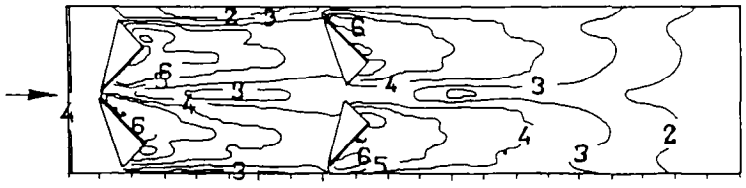

No.	1	2	3	4	5	6	7
α [W/(m^{2}K)]	9	11	13	16	21	30	50

FIG. 10. Local heat transfer coefficients on a channel wall with a delta winglet double row (Table 2) in staggered configuration, $\Delta y = B/2$, $Re = 4600$.

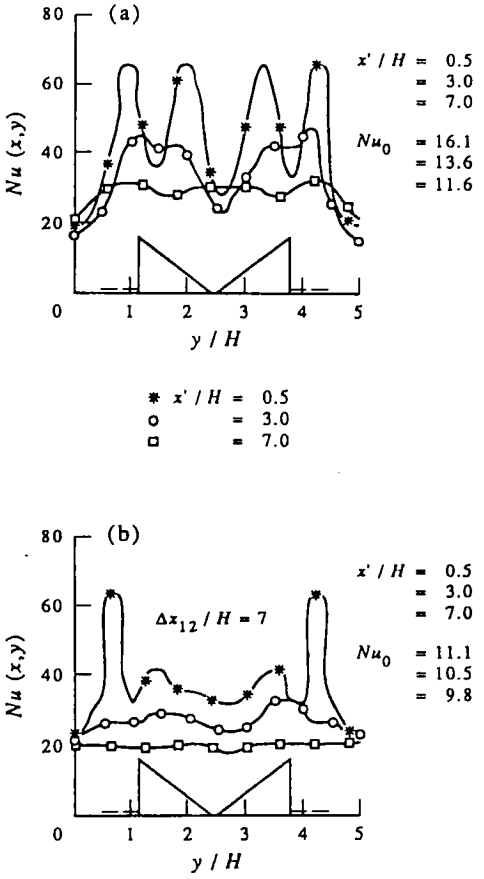

FIG. 11. Local spanwise Nusselt number distribution downstream of delta winglet pair (Table 2) for (a) first row, (b) aligned second row, $Re = 4600$, $\beta = 45^\circ$.

increases can be seen especially at the rear edges of the winglet stampings where new boundary layers start to grow, and behind the winglets showing the effect of the formation of longitudinal vortices. The distribution is qualitatively similar for the first and the second row.

The quantitative enhancements are shown in Fig. 11 as local spanwise Nusselt numbers at different cross-sections downstream of the first and the second winglet row for an aligned configuration. The plane duct (reference) values Nu_{xo} given in the figure have been calculated from a correlation (equation (6)), given in ref. [13, pp. 3.42] for constant wall temperature since exact measurements were not possible in channel flows with lengths of $L = 30H$ because of very low streamwise heat transfer gradients.

$$Nu_o = 7.55 + \frac{0.024x^{*-1.14}[0.0179Pr^{0.17}x^{*-0.64} - 0.14]}{[1.0 + 0.0358Pr^{0.17}x^{*-0.64}]^2} \quad (6)$$

for

$$10^{-4} < x^* < 10^{-1}; \quad x^* = \frac{x}{D_h Re\, Pr}.$$

The Nusselt number is based on the difference between the wall and the bulk temperatures at the respective streamwise position in contrast to the measured Nusselt numbers which are based on the difference between wall and entrance temperatures. Hence a direct comparison of the local streamwise values for plane channel flows and measurements shows smaller heat transfer enhancements than those that would result with the same reference temperature differences. This also holds for averaged and normalized values of Nu. The plane duct values are obtained at the sides of the investigated symmetry area directly downstream of the first winglet row. Local heat transfer enhancements are highest downstream of the second row, here values of nearly six times the plane duct value are found. Further downstream the distribution broadens and the large peaks disappear.

The structure of the heat transfer for staggered and aligned configurations are similar with regard to the number and position of the heat transfer peaks. This had been expected from the similar qualitative flow structure of the flow visualization.

Mean heat transfer and drag

The span averaged Nusselt numbers Nu_x normalized with the corresponding plane duct value N_{xo} for staggered and aligned configuration of delta winglet double rows, as given in Table 2 are compared in Fig. 12. Nu_x is defined by

$$Nu_x = \frac{1}{B}\int Nu(x,y)\,\mathrm{d}y|_{\mathrm{const}(x)}. \quad (8)$$

The figure shows that the distributions are nearly the same for aligned and staggered arrangements in the range $0 < x/H < 20$, the differences are of the order of the experimental error. For greater flow lengths the aligned arrangement is advantageous, the heat transfer is up to 10% higher than for the staggered winglets. The span averaged enhancement over the plane duct heat transfer is sufficiently higher at the second row since the plane duct value decreases rapidly downstream of the channel entrance. The peak enhancement value at the first winglet row is 150%,

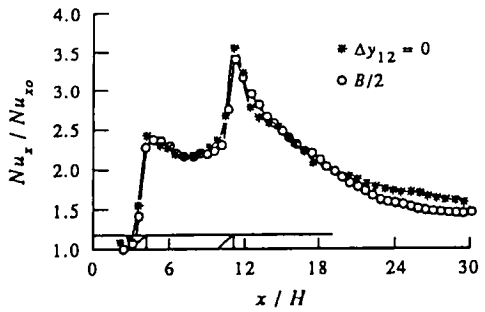

FIG. 12. Normalized span averaged Nusselt numbers Nu_x/Nu_{xo} for channel with delta winglet double row (Table 2) in staggered and aligned configuration, $\beta = 45^\circ$, $Re = 4600$.

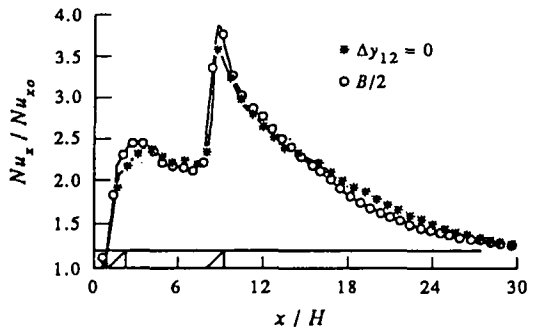

FIG. 13. Normalized span averaged Nusselt number Nu_x/Nu_{xo} for channel with delta winglet double row (Table 2) in staggered and aligned configuration, $\beta = 65°$, $Re = 4600$.

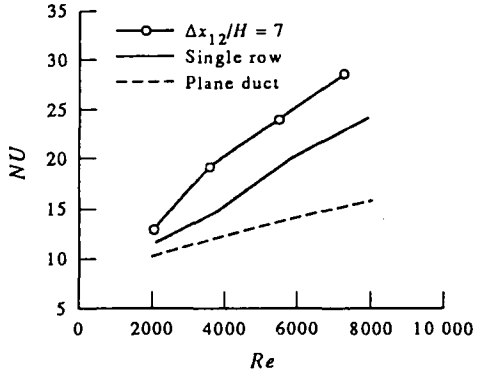

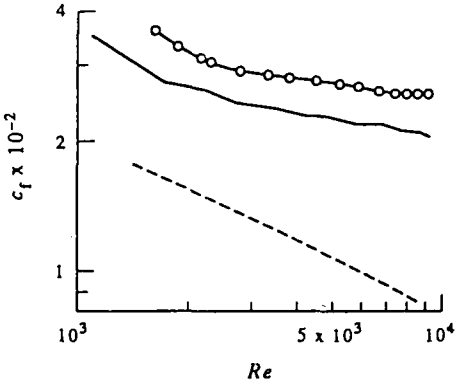

FIG. 14. Reynolds number dependence of global Nusselt number and drag coefficient for aligned delta winglet double row at $\beta = 45°$ (see Table 2).

at the second it is 250%. This indicates that for a double row arrangement of vortex generators the vortices of the oncoming flow can be beneficial for the vortex formation by the generators of the following row. The second row of delta winglets acts as boosters or amplifiers for the vortices in the oncoming flow. The streamwise decrease of the heat transfer enhancement is, however, stronger for the winglets in the second row than for the first row. At the channel exit ($x/H = 30$) the heat transfer is still increased by 50%.

The situation changes if the angle of attack of the winglets is supercritical, $\beta = 65°$, as shown in Fig. 13. The peak values at the winglets are comparable to those at $\beta = 45°$. The heat transfer decrease downstream of the second row is stronger than behind the $\beta = 45°$ winglets. At the rear end of the investigated channel area the heat transfer enhancement is only 23% over the plane duct value. Again the distributions are nearly identical for the in-line and staggered configurations, since for the supercritical flow the arrangement is not important.

The global Nusselt number for the complete channel wall ($A_f/A_{VG} = 37.5$) as well as the measured drag coefficient for the $\beta = 45°$ configuration are listed in Table 3. The global Nusselt number for the aligned configuration is 60% higher than for the plane channel; it is 5% higher than for the staggered arrangement just as is the drag coefficient. The ratio of the normalized coefficients for heat transfer and drag are nearly the same.

Table 3. Global Nusselt number and drag coefficient for staggered and aligned delta winglet rows (Table 2), $\beta = 45°$, $Re = 4600$

	Aligned Configuration	Staggered Configuration
	$\Delta y = 0$	$\Delta y = B/2$
NU	20.5	19.5
NU/NU_o	1.6	1.52
$c_F [10^{-2}]$	2.73	2.54
c_F/c_{Fo}	2.45	2.29

For the more advantageous aligned arrangement the dependence of global heat transfer and drag on the Reynolds number is shown in Fig. 14. The figure shows also the behavior of the plane duct and the channel with only a single delta winglet row.

The heat transfer increases nearly linearly with the Reynolds number; its enhancement over the plane duct is higher for high Reynolds numbers. For Reynolds numbers of about 6000 an enhancement of 80% was stated. The drag coefficient tends to be nearly constant with growing Reynolds number whereas the plane duct value strongly decreases. The ratio of global heat transfer and drag each normalized with its plane duct value is shown in Table 4 for the aligned double row results of Fig. 14. The table shows that the ratio is higher for high Reynolds numbers, there the winglets are more effective.

CONCLUSIONS

Stacks of parallel plates forming channels with punched out delta winglet pairs as longitudinal vortex generators have been investigated experimentally for

Table 4. Ratio of normalized Nusselt number and drag coefficient for single and double delta winglet row of Fig. 14

	$(NU/NU_o)/(c_F/c_{F_o})$	
Re	Single	Aligned double row
2000	0.60	0.62
4000	0.64	0.64
6000	0.66	0.67
8000	0.66	0.67

heat transfer enhancement of compact heat exchangers. Qualitative studies of the flow structure, local and mean heat transfer measurements on the channel walls of the configuration, and drag measurements have been performed in a small wind tunnel by flow visualization, unsteady liquid crystal thermography, and balancing, respectively. Aligned and staggered double-row configurations of delta winglet pairs have been investigated. The qualitative flow structure, the number of developing vortices per vortex generator, and their streamwise development have been nearly independent of the vortex generator arrangement. The vortices in the wake of the second row show more unsteadiness than the first row vortices. The critical value of the angle of attack is $\beta_{crit} \approx 55^\circ$ for the second row whereas it is $\beta_{crit} \approx 70^\circ$ for the first row. Behind the second row of winglets in aligned configuration the local heat transfer enhancement normalized by the plane duct value is higher than for the first row. Highest heat transfer was achieved for angles of attack near the critical value. Aligned double rows of delta winglets give slightly higher heat transfer than staggered double rows. Local heat transfer enhancements of more than 300% can be observed for angles of attack $\beta = 45^\circ$; the average heat transfer enhancement for $Re = 6000$ was 80% on a channel wall whose area was 37.5 times the winglet area. The drag simultaneously increases with 165%. The ratio of heat transfer enhancement and drag increase each normalized with the plane duct value is about 0.6 and grows with increasing Reynolds number. The global convective heat transfer on the fins can be augmented substantially by means of longitudinal vortex generators by modifying less than 3% of the heat transfer surface.

REFERENCES

1. W. M. Kays and A. L. London, *Compact Heat Exchangers* (2nd Edn). McGraw-Hill, New York (1984).
2. F. J. Edwards and C. J. R. Alker, The improvement of forced surface heat transfer using protrusions in the form of cubes and vortex generators, *5th IHTC* Vol. 2, Tokyo, pp. 244-248 (1974).
3. C. M. B. Russell, T. V. Jones and G. H. Lee, Heat transfer enhancement using vortex generators, *7th IHTC* Vol. 3, München, pp. 283–288 (1982).
4. M. Fiebig, U. Brockmeier, N. K. Mitra and T. Güntermann, Structure of velocity and temperature fields in laminar channel flows with longitudinal vortex generators, *Num. Heat Transfer, Part A* **15**, 281–302 (1989).
5. A. Y. Turk and G. H. Junkhan, Heat transfer enhancement downstream of vortex generators on a flat plate, *8th IHTC* Vol. 6, San Francisco, pp. 2903–2908 (1986).
6. M. Fiebig, P. Kallweit and N. K. Mitra, Wing type vortex generators for heat transfer enhancement, *8th IHTC* Vol. 6, San Francisco, pp. 2908–2913 (1986).
7. M. Fiebig, P. Kallweit, N. K. Mitra and S. Tiggelbeck, Heat transfer enhancement and drag by longitudinal vortex generators in channel flow, *ETF Science* **4**, 103–114 (1991).
8. S. Tiggelbeck, N. K. Mitra and M. Fiebig, Flow structure and heat transfer in a channel with multiple longitudinal vortex generators. In *Proc. Second World Conf. on Experimental Heat Transfer, Fluid Mechanics and Thermodynamics* (Edited by J. F. Keffer, R. K. Shah, E. N. Ganic), June 1991. Elsevier, Dubrovnik (pp. 126–133).
9. P. T. Ireland and T. V. Jones, Detailed measurements of heat transfer on and around a pedestal in fully developed passage flow, *8th IHTC* Vol. 3, San Francisco, pp. 975–980 (1986).
10. R. J. Moffat, Describing the uncertainties in experimental results, *ETF Science* **1**, 3–17 (1988).
11. S. Tiggelebeck, Experimentelle Untersuchungen an Kanalströmungen mit Einzel- und Doppel-Wirbelerzeugerreihen für den Einsatz in kompakten Wärmetauschern, *VDI-Fortschritt-Bericht*, Reihe 19, Nr 49 (1991).
12. U. Brockmeier, Numerisches Verfahren zur Berechung dreidimensionaler Strömungs- und Temperaturfelder. Dissertation, Inst. Thermo-Fluiddynamik, Ruhr-Universität Bochum (1987).
13. S. Kakac, R. K. Shah and W. Aung (Eds), *Handbook of Single-phase Convective Heat Transfer*. John Wiley, New York (1987).